Available online at www.sciencedirect.com
SCIENCE DIRECT®
Journal of Sound and Vibration 287 (2005) 883–900
JOURNAL OF SOUND AND VIBRATION
www.elsevier.com/locate/jsvi

Reliability-based critical earthquake load models. Part 2: nonlinear structures

A.M. Abbas, C.S. Manohar*

Department of Civil Engineering, Indian Institute of Science, Bangalore 560012, India

Received 13 January 2004; received in revised form 6 September 2004; accepted 6 December 2004
Available online 17 February 2005

Abstract

The problem of determining critical stochastic earthquake excitation models for simple nonlinear systems under single-point or multi-point nonstationary seismic inputs is considered. The earthquake acceleration components are obtained by multiplying known deterministic enveloping functions with zero mean Gaussian stationary random processes with unknown auto-power spectral density functions (for single-point excitations) and power spectral density matrix (for multi-point excitations). The definition of critical earthquake input is based on the notion of a performance function. The system is considered to have failed if the maximum response over a given time interval exceeds specified limits. The critical excitations are defined as those that minimize the Hasofer–Lind reliability index associated with this performance function. The computation of this index, in turn, is based on the use of response surface to model the limit surface near the check point. Here the quantity to be optimally determined is taken to be the unknown input power spectral density function (for single-point excitations) or the input power spectral density matrix (for multi-point excitations). The excitations are taken to satisfy constraints on total average energy, zero crossing rate, lower bounds on entropy rate and other positivity and bounding requirements that are of mathematical nature. The resulting constrained nonlinear optimization problems are solved using the sequential quadratic programming method. Illustrative examples for computing random critical excitations for singly supported and multiply supported oscillators that have cubic force–displacement relations are provided.

*Corresponding author. Tel.: +91 80 2293 3121; fax: +91 80 2360 0404.
E-mail addresses: amabbas@mail.com (A.M. Abbas), manohar@civil.iisc.ernet.in (C.S. Manohar).

0022-460X/$ - see front matter © 2005 Elsevier Ltd. All rights reserved.
doi:10.1016/j.jsv.2004.12.003

1. Introduction

Critical earthquake excitations, by definition, depend upon properties of the structure considered and site soil conditions. The problem of determination of critical earthquake excitations for linear structures is widely studied; see, the accompanying paper [1] for relevant references. On the other hand, the problem of determining critical earthquake excitations including the effects of structural nonlinearities has been studied to a very limited extent in the existing literature. Given that the treatment of structural nonlinearities constitutes one of the central themes in earthquake resistant design, it is of significant interest to develop methods for computing critical earthquake load models for these structures. Early studies in this area of research are due to Iyengar [2] and Drenick [3]. Iyengar [2] considered inputs having known total energy and obtained critical excitations for a class of nonlinear systems in terms of an associated linear system. He also treated the input total energy as a random variable and obtained the worst possible distribution of the critical response. By linearizing the given nonlinear system, Drenick [3] has obtained critical excitations in terms of impulse response of linearized equations. Philippacopoulos and Wang [4] developed critical inelastic response spectra using recorded ground accelerograms as basis functions in a series representation for the critical seismic excitation. Westermo [5] has defined critical response in terms of input energy to the system and has found critical excitations for linear, elasto-plastic and hysteretic single-degree-of-freedom (sdof) systems using calculus of variations. Pirasteh et al. [6] have computed the critical excitations for inelastic multi-story frame structures under deterministic earthquake inputs. The response variable for maximization was chosen as the cumulative inelastic energy dissipation or sum of inter-story drifts. The masters theses by Ravi [7] and Srinivas [8] explored the use of equivalent linearization in determining critical power spectral density (psd) matrix models for multiply-supported nonlinear systems under spatially varying random seismic support motions. More recently, Takewaki [9,10] has developed critical input psd function models for earthquake inputs to sdof and mdof elastic–plastic systems. This analysis employs the method of statistical linearization to approximately evaluate the structure response. The variable of optimization in these two studies has been the sum of the response standard deviations of inter-story drifts normalized to yield drifts.

In the companion paper [1] the present authors have investigated the nature of random critical excitations for linear systems that are tailored to maximize the probability of failure defined on the event of highest response over a given duration exceeding specified limits. The formulations presented therein is not directly applicable to problems of nonlinear systems because of the significant difficulty involved in determining the extreme value distribution of nonlinear structural response. One alternative to deal with this difficulty is to adopt statistical linearization to approximate the nonlinear structural response by equivalent Gaussian responses. Another alternative is to explore if methods of time-variant structural reliability analysis could be employed to achieve this objective. It is the latter option that the present study adopts. Specifically, the present study explores the use of response surface modelling in determining critical random excitations for simple nonlinear oscillators. See, for example, the papers by Faravelli [11], Bucher and Bourgund [12] and Rajashekhar and Ellingwood [13] for a basic exposition of the response surface modelling in structural reliability analysis. Attention in the present study is focussed on doubly supported sdof oscillators with nonlinear force–displacement characteristics. The supports are taken to undergo earthquake-induced differential motions. The ground accelerations are modelled as a vector of nonstationary Gaussian random processes with each component obtained as a product of a specified envelope function and an unknown stationary Gaussian random process with

zero mean. The psd matrix of the stationary part of the input vector is optimally determined such that a measure of structural reliability, expressed in terms of the response over a given time interval, being less than a specified permissible limit, is minimized. In computing this reliability, attention is limited to performance functions involving single response variables. Furthermore, the input is constrained to possess specified total average energy, average zero crossing rate and a measure of disorder expressed in terms of input entropy rate. The present study applies the response surface method as developed by Bucher and Bourgund [12] to arrive at the measure of reliability expressed in terms of the Hasofer–Lind reliability index. Illustrative examples on sdof systems with cubic force–displacement characteristics are included and these examples clearly bring out the influence that the structural nonlinearity has on the definition of the critical earthquake inputs.

2. Nonlinear sdof system under random support motions

A doubly supported sdof system subject to differential support motions is shown in Fig. 1. Here m is the oscillator mass; c_1, c_2 the damping coefficients; k_1, k_2 the linear spring constants and α_1, α_2 the nonlinear spring constants. This system can serve as an idealization for a doubly-supported building frame or a single span extended pipe or a bridge structure. For the purpose of illustration, we model the spring stiffness to possess cubic force–displacement characteristics. Accordingly, for a displacement Δ, the force develops in the left spring would be of the form $k_1\Delta + \alpha_1\Delta^3$. This type of systems are believed to serve well as archetypal nonlinear systems suited for the development work such as the one being reported herein. The equation governing the total displacement $x(t)$ can be shown to be given by

$$m\ddot{x} + c_1(\dot{x} - \dot{x}_g) + k_1(x - x_g) + \alpha_1(x - x_g)^3 + c_2(\dot{x} - \dot{y}_g) + k_2(x - y_g) + \alpha_2(x - y_g)^3 = 0. \tag{1}$$

Here a dot represents differentiation with respect to time t and, $x_g(t)$, $y_g(t)$ and $\dot{x}_g(t)$, $\dot{y}_g(t)$ represent the ground displacements and velocities at the support points A and B, respectively (Fig. 1). The above equation can be recast in terms of the linear structure natural frequency, ω, and damping ratio, ζ, as follows:

$$\begin{aligned} &\ddot{x} + 2\zeta\omega\dot{x} + (\omega^2 + 3\varepsilon_1 x_g^2 + 3\varepsilon_2 y_g^2)x - 3(\varepsilon_1 x_g + \varepsilon_2 y_g)x^2 + \varepsilon x^3 \\ &\quad = \varepsilon_1 x_g^3 + \varepsilon_2 y_g^3 + \frac{\omega^2}{k}(c_1\dot{x}_g + c_2\dot{y}_g + k_1 x_g + k_2 y_g), \\ &\varepsilon_1 = \frac{\alpha_1}{m} = \alpha_1\frac{\omega^2}{k}, \quad \varepsilon_2 = \frac{\alpha_2}{m} = \alpha_2\frac{\omega^2}{k}, \quad \varepsilon = \varepsilon_1 + \varepsilon_2. \end{aligned} \tag{2}$$

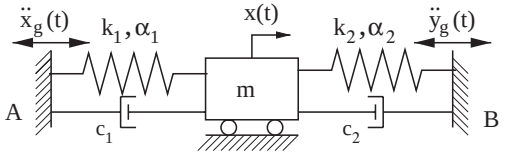

Fig. 1. Example structure considered.

Thus it follows that the governing equation of motion in this case is not only nonlinear but also has parametric excitation terms. Furthermore, the external excitations, as well as the parametric excitation terms, appearing in the above equation, contain squares and cubes of Gaussian random processes. This would mean that the system receives non-Gaussian inputs both parametrically and externally.

It may be noted that if the two supports are subject to identical displacements, Eq. (2) assumes a simpler form given by

$$m\ddot{x} + (c_1 + c_2)(\dot{x} - \dot{x}_g) + (k_1 + k_2)(x - x_g) + (\alpha_1 + \alpha_2)(x - x_g)^3 = 0. \tag{3}$$

Thus, with the substitution $y = x - x_g$ for the relative displacement, this equation can be transformed into

$$\ddot{y} + 2\eta\omega\dot{y} + \omega^2 y + (\varepsilon_1 + \varepsilon_2)y^3 = -\ddot{x}_g. \tag{4}$$

This equation represents the well known Duffing's oscillator with excitation $-\ddot{x}_g(t)$. It is important to note that, in contrast to Eq. (2), this equation does not contain parametric excitation terms, and the excitation is Gaussian, and, therefore, represents a relatively simpler situation. In the discussion to follow, we present the formulation of critical excitation models with respect to the more general case of Eq. (2). This formulation can be straightforwardly be modified to dealing with the simpler situation of $x_g(t) = y_g(t)$ (Eq. (4)).

We represent the support motions as $\ddot{x}_g(t) = e_x(t)\ddot{w}_g(t)$ and $\ddot{y}_g(t) = e_y(t)\ddot{v}_g(t)$. Here $e_x(t)$ and $e_y(t)$ are the enveloping functions that are taken to be known and $\ddot{w}_g(t)$ and $\ddot{v}_g(t)$ are zero mean jointly stationary Gaussian random processes with an unknown psd matrix $\mathbf{S}(\omega)$. In this study, we propose to determine $\mathbf{S}(\omega)$ such that it maximizes the probability of exceedance of the force in one of the springs beyond its load carrying capacity R. Herein, we treat R as a random variable with prescribed probability density function. Mathematically, the problem of determining the input critical psd matrix can be stated as finding $\mathbf{S}(\omega)$ that maximizes $P_f = P[R - k_1 \max_{0<t<\infty} |[x(t) - x_g(t)] + (\varepsilon_1/\omega^2)[x(t) - x_g(t)]^3| < 0]$, subject to a set of constraints that are reflective of known features of earthquake input. As has been done in Part 1 of this paper [1], these constraints are taken to represent known values of total energy, E_{0x}, E_{0y}, zero crossing rate, n^+_{0x}, n^+_{0y}, and lower limits on entropy rate, $\Delta\bar{H}_{Wx}, \Delta\bar{H}_{Wy}$. Here, the subscripts x and y denote, respectively, quantities associated with the left and the right supports. The determination of critical input psd matrix, according to this definition, requires the ability to evaluate the structure probability of failure, P_f, as given above. In this context, it is important to note that methods to evaluate, in an exact manner, the probability distribution function of the quantity $k_1 \max_{0<t<\infty} |[x(t) - x_g(t)] + (\varepsilon_1/\omega^2)[x(t) - x_g(t)]^3|$ are not currently available. To proceed further, we adopt response surface methods to assess the structure probability of failure [11–13]. To facilitate this, the stationary components of the support accelerations are represented as

$$\ddot{w}_g(t) = \sum_{n=1}^{N_f} \{A_n \cos\, \Omega_n t + B_n \sin\, \Omega_n t\},$$

$$\ddot{v}_g(t) = \sum_{n=1}^{N_f} \{C_n \cos\, \Omega_n t + D_n \sin \Omega_n t\}. \tag{5}$$

Here $\{A_n, B_n, C_n, D_n\}_{n=1}^{N_f}$ is a set of $4N_f$ zero mean Gaussian random variables and N_f is the number of discrete frequencies included in the series representation for $\ddot{w}_g(t)$ and $\ddot{v}_g(t)$ within (ω_0, ω_c). Since the processes $\ddot{w}_g(t)$ and $\ddot{v}_g(t)$ are taken to be jointly stationary, it is required that

$$\begin{aligned}&\langle A_m A_n\rangle = \langle B_m B_n\rangle = \sigma_{wn}^2\delta_{mn}, \langle C_m C_n\rangle = \langle D_m D_n\rangle = \sigma_{vn}^2\delta_{mn},\\ &\langle A_m B_n\rangle = \langle C_m D_n\rangle = 0, \quad \forall m, n = 1, 2, \ldots, N_f\end{aligned} \tag{6}$$

and

$$\begin{aligned}&\langle A_m C_n\rangle = \langle B_m D_n\rangle = \sigma_{ACn}\delta_{mn},\\ &\langle A_m D_n\rangle = -\langle B_m C_n\rangle = \sigma_{ADn}\delta_{mn}, \quad \forall m, n = 1, 2, \ldots, N_f.\end{aligned} \tag{7}$$

In the above equations $\langle . \rangle$ denotes the mathematical expectation operator. It is to be emphasized that, the conditions given by Eq. (6) imply that the processes $\ddot{w}_g(t)$ and $\ddot{v}_g(t)$ are individually stationary, while those of Eq. (7) ensure that $\ddot{w}_g(t)$ and $\ddot{v}_g(t)$ are jointly stationary. Accordingly, the auto and cross-covariance functions of these processes can be shown to be given, respectively, by

$$\begin{aligned}R_{ww}(\tau) = \sum_{n=1}^{N_f} \sigma_{wn}^2 \cos\,\Omega_n\tau, R_{vv}(\tau) = \sum_{n=1}^{N_f} \sigma_{vn}^2 \cos\,\Omega_n\tau,\\ R_{wv}(\tau) = \sum_{n=1}^{N_f} \{\sigma_{ACn} \cos\,\Omega_n\tau + \sigma_{ADn} \sin\Omega_n\tau\}.\end{aligned} \tag{8}$$

It follows that $R_{ww}(\tau) = R_{ww}(-\tau)$, $R_{vv}(\tau) = R_{vv}(-\tau)$ and $R_{wv}(\tau) = R_{vw}(-\tau)$. The ground velocities and displacements appearing in Eq. (2) are computed as

$$\begin{aligned}\dot{x}_g(t) = &\sum\nolimits_{n=1}^{N_f} \int_0^t e_x(\tau)[A_n \cos\Omega_n\tau + B_n \sin\,\Omega_n\tau]\,\mathrm{d}\tau\\ &- \sum_{n=1}^{N_f} \int_0^\infty e_x(\tau)[A_n \cos\Omega_n\tau + B_n \sin\Omega_n\tau]\,\mathrm{d}\tau,\\ \dot{y}_g(t) = &\sum_{n=1}^{N_f} \int_0^t e_y(\tau)[C_n \cos\Omega_n\tau + D_n \sin\Omega_n\tau]\,\mathrm{d}\tau\\ &- \sum_{n=1}^{N_f} \int_0^\infty e_y(\tau)[C_n \cos\Omega_n\tau + D_n \sin\Omega_n\tau]\,\mathrm{d}\tau,\\ x_g(t) = &\sum_{n=1}^{N_f} \int_0^t e_x(\tau)(t-\tau)[A_n \cos\Omega_n\tau + B_n \sin\Omega_n\tau]\,\mathrm{d}\tau - t\\ &\sum_{n=1}^{N_f} \int_0^\infty e_x(\tau)[A_n \cos\Omega_n\tau + B_n \sin\Omega_n\tau]\,\mathrm{d}\tau,\end{aligned}$$

$$y_g(t) = \sum_{n=1}^{N_f} \int_0^t e_y(\tau)(t-\tau)[C_n \cos \Omega_n \tau + D_n \sin \Omega_n \tau]\, \mathrm{d}\tau - t \sum_{n=1}^{N_f} \int_0^\infty e_y(\tau)[C_n \cos \Omega_n \tau + D_n \sin \Omega_n \tau]\, \mathrm{d}\tau. \tag{9}$$

In deriving these expressions, the conditions $x_g(0) = 0$, $\lim_{t\to\infty} \dot{x}_g(t) \to 0$, $y_g(0) = 0$ and $\lim_{t\to\infty} \dot{y}_g(t) \to 0$ are employed. To proceed further, we now introduce the performance function

$$g(\mathbf{X}) = R - k_1 \max_{0<t<\infty} |[x(t) - x_g(t)] + \frac{\varepsilon_1}{\omega^2}[x(t) - x_g(t)]^3| \tag{10}$$

such that the structure failure probability is given by $P_f = P[g(\mathbf{X}) < 0]$. Here $\mathbf{X} = [R, \{A_n, B_n, C_n, D_n\}_{n=1}^{N_f}]^{\mathrm{t}}$ is the vector of the basic random variables inclusive of load and resistance characteristics. It is to be noted that in the above equation terms involving $x(t) - y_g(t)$ do not appear explicitly; it is however, emphasized that $x(t)$ still depends upon $y_g(t)$ in an implicit manner. It must also be noted that, an expression for $g(\mathbf{X})$ in terms of $\mathbf{X}$ is available only in an implicit form via the governing equation of motion. This necessitates the use of methods such as response surface modelling to approximately evaluate P_f. In the present study we propose to use the response surface method as developed by Bucher and Bourgund [12]. This procedure leads to a quadratic fit to the limit surface near the design point and yields a measure of structural reliability defined in terms of the Hasofer–Lind reliability index. The problem of computing critical earthquake excitations can thus be stated as finding the variables $\{\sigma_{wn}^2, \sigma_{vn}^2, \sigma_{ACn}, \sigma_{ADn}\}_{n=1}^{N_f}$ that minimize the structure reliability index under the following constraints:

$$\begin{aligned}
&\sum_{n=1}^{N_f} \sigma_{wn}^2 = E_{0x}, \quad \sum_{n=1}^{N_f} \sigma_{vn}^2 = E_{0y},\\
&\sum_{n=1}^{N_f} \sigma_{wn}^2 \Omega_n^2 = E_{2x}, \quad \sum_{n=1}^{N_f} \sigma_{vn}^2 \Omega_n^2 = E_{2y},\\
&\sigma_{ACn}^2 + \sigma_{ADn}^2 < \sigma_{wn}^2 + \sigma_{vn}^2,\\
&\sigma_{wn}^2 > 0, \quad \sigma_{vn}^2 > 0, \quad n = 1, 2, ..., N_f,\\
&\frac{1}{2(\omega_c - \omega_0)} \sum_{n=1}^{N_f} (\Omega_n - \Omega_{n-1}) \log_e \left[1.0 + \frac{\sigma_{wn}^2}{S_0(\Omega_n - \Omega_{n-1})}\right] \geqslant \Delta \bar{H}_{Wx},\\
&\frac{1}{2(\omega_c - \omega_0)} \sum_{n=1}^{N_f} (\Omega_n - \Omega_{n-1}) \log_e \left[1.0 + \frac{\sigma_{vn}^2}{S_0(\Omega_n - \Omega_{n-1})}\right] \geqslant \Delta \bar{H}_{Wy}.
\end{aligned} \tag{11}$$

It can be shown that the constraints $\sigma_{ACn}^2 + \sigma_{ADn}^2 < \sigma_{wn}^2 + \sigma_{vn}^2$ for $n = 1, ..., N_f$ ensures that the covariance matrix of the random variables A_n, B_n, C_n and D_n is positive definite $\forall n = 1, 2, ..., N_f$. Clearly, the problem of finding the critical input psd matrix constitutes a constrained nonlinear optimization problem. As in Part 1 of the study [1] we employ the sequential quadratic programming method to treat this problem.

3. Determination of critical psd matrix using response surface models

The performance function, as given by Eq. (10), is defined in a space of $4N_f + 1$ random variables denoted collectively by the vector $\mathbf{X}$. The first step in implementing the response surface method for reliability computation consists of transforming the basic random variables $\mathbf{X}$ into a vector of standard normal random variables denoted by $\mathbf{Y}$. The essence of the response surface method consists of replacing the implicit performance function given in Eq. (10) by an approximating quadratic surface [12]

$$\bar{g}(\mathbf{Y}) = a + \sum_{i=1}^{N_{rv}} b_i Y_i + \sum_{i=1}^{N_{rv}} c_i Y_i^2. \tag{12}$$

Here $N_{rv} = 4N_f + 1$ is the number of basic random variables on which the performance function depends and $a, \{b_i\}_{i=1}^{N_{rv}}, \{b_i\}_{i=1}^{N_{rv}}$ are the unknown deterministic parameters to be determined. It must be noted here that the problem of determination of the Hasofer–Lind reliability index β_{HL} itself constitutes a constrained nonlinear optimization problem. This optimization problem, in turn, is embedded into the optimization problem associated with the determination of the critical psd matrix parameters. Consequently, the algorithm proposed in the present study, for computing the critical input psd matrix, has two optimization routines. The first routine is meant for computing the critical excitations, while the second subroutine, that computes β_{HL}, is called by the main routine at each major step of computing the critical input. The steps involved in these calculations are as follows:

(1) Select a failure criterion for the structure, fix R, define mean and variance of the basic random variables, $\{\mu_i, \sigma_i^2\}_{i=1}^{N_{rv}}$, and make an initial guess for the optimization variables $\{\sigma_{wn}^2, \sigma_{vn}^2, \sigma_{ACn}, \sigma_{ADn}\}_{n=1}^{N_f}$.
(2) Define the performance function $g(R, \{A_n, B_n, C_n, D_n\}_{n=1}^{N_f})$ as given by Eq. (10).
(3) Make an initial guess for the failure point $\{x_{i0}^*\}_{i=1}^{N_{rv}}$, compute the corresponding point in the standard uncorrelated normal space, $\{y_{i0}^*\}_{i=1}^{N_{rv}}$. Here the transformation $\mathbf{Y} = \mathbf{T}^{\mathrm{t}}\mathbf{X}'$ is used, where, $X_i' = (X_i - \mu_i)/\sigma_i$, is the reduced variate and $\mathbf{T}$ is an orthogonal transformation matrix. The details of this transformation are provided in the book by Ang and Tang [14].
(4) Call the basic optimization routine that provides new values for $\{\sigma_{wn}^2.\ \sigma_{vn}^2, \sigma_{ACn}, \sigma_{ADn}\}_{n=1}^{N_f}$.
(5) Fit a response surface in the uncorrelated standard normal space. Thus the actual implicit performance function, $g(\mathbf{Y})$, is approximated with a closed-form function $\bar{g}(\mathbf{Y})$ at the failure point. In the present work, we use a quadratic polynomial function as given in Eq. (12) [12]. The steps of this fitting are summarized as follows:

- Sample Y in Eq. (12) at $2N_{rv} + 1$ points, that is, at mean, $\bar{\mu}_i$, and mean $\pm f\bar{\sigma}_i$ of these random variables. Here f is a constant and $\bar{\mu}_i = 0$, $\bar{\sigma}_i = 1$ are mean and standard deviation of Y_i, respectively.
- Evaluate the actual performance function, $g(\mathbf{Y})$ at the $2N_{rv} + 1$ points. Here the quantity $\max_{0<t<\infty}|[x(t, R, A_n, B_n, C_n, D_n) - x_g(t, A_n, B_n, C_n, D_n)] + (\varepsilon_1/\omega^2)[x(t, R, A_n, B_n, C_n, D_n) - x_g(t, A_n, B_n, C_n, D_n)]^3|$, $n = 1, 2, ..., N_f$, is computed using numerical integration of the governing equations of motion.

- Solve the set of $2N_{rv}+1$ algebraic equations given by $\mathbf{AB}=\mathbf{G}$, to compute the values of the variables $\{a, b_i, c_i\}_{i=1}^{N_{rv}}$. Here, the matrix $\mathbf{A}$ is of size $2N_{rv}+1$ by $2N_{rv}+1$, the matrices $\mathbf{B}$ and $\mathbf{G}$ are of the size $2N_{rv}+1$ by 1, and these matrices are given as

$$\mathbf{A}=\begin{bmatrix}
1 & \bar{\mu}_1 & \bar{\mu}_2 & \dots & \bar{\mu}_{N_{rv}} & \bar{\mu}_1^2 & \bar{\mu}_2^2 & \dots & \bar{\mu}_{N_{rv}}^2 \\
1 & \bar{\mu}_1+f\bar{\sigma}_1 & \bar{\mu}_2 & \dots & \bar{\mu}_{N_{rv}} & (\bar{\mu}_1+f\bar{\sigma}_1)^2 & \bar{\mu}_2^2 & \dots & \bar{\mu}_{N_{rv}}^2 \\
1 & \bar{\mu}_1 & \bar{\mu}_2+f\bar{\sigma}_2 & \dots & \bar{\mu}_{N_{rv}} & \bar{\mu}_1^2 & (\bar{\mu}_2+f\bar{\sigma}_2)^2 & \dots & \bar{\mu}_{N_{rv}}^2 \\
 & & & & & & & & \\
1 & \bar{\mu}_1 & \bar{\mu}_2 & \dots & \bar{\mu}_{N_{rv}}+f\bar{\sigma}_{N_{rv}} & \bar{\mu}_1^2 & \bar{\mu}_2^2 & \dots & (\bar{\mu}_{N_{rv}}+f\bar{\sigma}_{N_{rv}})^2 \\
1 & \bar{\mu}_1-f\bar{\sigma}_1 & \bar{\mu}_2 & \dots & \bar{\mu}_{N_{rv}} & (\bar{\mu}_1-f\bar{\sigma}_1)^2 & \bar{\mu}_2^2 & \dots & \bar{\mu}_{N_{rv}}^2 \\
1 & \bar{\mu}_1 & \bar{\mu}_2-f\bar{\sigma}_2 & \dots & \bar{\mu}_{N_{rv}} & \bar{\mu}_1^2 & (\bar{\mu}_2-f\bar{\sigma}_2)^2 & \dots & \bar{\mu}_{N_{rv}}^2 \\
 & & & & & & & & \\
1 & \bar{\mu}_1 & \bar{\mu}_2 & \dots & \bar{\mu}_{N_{rv}}-f\bar{\sigma}_{N_{rv}} & \bar{\mu}_1^2 & \bar{\mu}_2^2 & \dots & (\bar{\mu}_{N_{rv}}-f\bar{\sigma}_{N_{rv}})^2
\end{bmatrix}, \tag{13}$$

$$\mathbf{B}=[ab_1b_2\dots b_{N_{rv}}c_1c_2\dots c_{N_{rv}}]^{\mathrm{t}}, \quad \mathbf{G}=[g_1(\mathbf{X}')g_2(\mathbf{X}')g_3(\mathbf{X}')\dots g_{2N_{rv}+1}(\mathbf{X}')]^{\mathrm{t}}.$$

(6) Use the explicit limit surface $\bar{g}(\mathbf{Y})$ to calculate the reliability index, β_{HL}, and design point $\{y_i^*\}_{i=1}^{N_{rv}}$. The procedures of the subroutine that is involved in computing β_{HL}, are summarized as follows:

(a) Using the design point $\{y_i^*\}_{i=1}^{N_{rv}}$, compute β_{HL} as the shortest distance from the origin

$$\beta_{HL}=\sqrt{y^{*\mathrm{t}}y^*} \tag{14}$$

and evaluate also the value of the performance function, at the design point $\bar{g}(y^*)$.

(b) Compute the partial derivatives $\partial\bar{g}/\partial Y_i$ at the design point, $\{y_i^*\}_{i=1}^{N_{rv}}$.

(c) Update the design point and compute the unit vector α at the check point as follows:

$$y_{j+1}^*=\frac{1}{|\nabla\bar{g}(y_j^*)|^2}[\nabla\bar{g}(y_j^*)^{\mathrm{t}}y_j^*-\bar{g}(x_j^*)]\nabla\bar{g}(y_j^*), \quad \alpha_i=\frac{\partial\bar{g}/\partial Y_i}{\sqrt{\sum_{i=1}^{N_{rv}}(\partial\bar{g}/\partial Y_i)^2}}\bigg|_{Y_i=y_i^*}. \tag{15}$$

(d) Re-evaluate the reliability index, β_{HL}, using the new updated design point through Eq. (14).

(e) Check the convergence criteria for the β_{HL} algorithm, $|\beta_{HL_j}-\beta_{HL_{j-1}}|\leqslant\delta_1$ and $|g_j(\mathbf{Y})|\leqslant\delta_2$. Here δ_1 and δ_2 are small quantities to be selected. If both the convergence criteria are satisfied, stop the β_{HL} algorithm. Otherwise, repeat steps (a)–(e) until convergence is achieved.

(7) Update the starting point, $\{\bar{\mu}_i\}_{i=1}^{2N_{rv}+1}$ to $\{y_{M_i}\}_{i=1}^{2N_{rv}+1}$ as $y_{M_i}=\bar{\mu}_i+(y_i^*-\bar{\mu}_i)g(\bar{\mu}_i)(g(\bar{\mu}_i)-g(y_i^*))$ and re-fit a new response surface using the new updated point.

(8) Check convergence of the basic optimization routine, $|g_j(Y)\leqslant\delta_2|$, $|\sigma_{wn_{j+1}}^2-\sigma_{wn_j}^2|\leqslant\delta_3$, …, $|\sigma_{ADn_{j+1}}-\sigma_{ADn_j}^2|\leqslant\delta_3$. If convergence is achieved go to next step, if not go to step 4.

(9) Store the quantities, $\{\sigma_{wn}^2,\sigma_{vn}^2,\sigma_{ACn},\sigma_{ADn}\}_{n=1}^{N_f}$, β_{HL}, $\{x_i^*\}_{i=1}^{N_{rv}}$ and $\{\alpha_i\}_{i=1}^{N_{rv}}$.

It is of interest to note that the formulation of critical excitations in terms of optimal reliability indices, as developed above, leads to the following input-response descriptors:

- Critical psd matrix that produces the least β_{HL} that is compatible with a set of specified constraints.
- The reliability index, β_{HL}, associated with the critical input as obtained above.
- A notional probability of failure, given by $P_{f_0} = \Phi(-\beta_{HL})$, associated with the performance function considered. Here, $\Phi(\cdot)$ is the Gaussian probability distribution function.
- A check point which characterizes a single time history that leads to maximum likelihood of failure.
- A vector $\{\gamma_i\}_{i=1}^{4N_f}$ which is a measure of sensitivity of reliability index with respect to individual random variables $\{A_i, B_i, C_i, D_i\}_{i=1}^{N_f}$. Since the design point can be expressed as $y_i^* = -\beta_{HL}\alpha_i$, it follows that $\alpha_i = -\partial\beta_{HL}/\partial y_i^*$. Following Kiureghian and Ke [15] it can be shown that the sensitivity vector, $\{\gamma_i\}_{i=1}^{4N_f}$, is expressible in terms of $\{\alpha_i\}_{i=1}^{4N_f}$ as $\gamma = (\sigma\mathbf{J}_{\mathbf{Y},\mathbf{X}}\alpha)|\sigma\mathbf{J}_{\mathbf{Y},\mathbf{X}}\alpha|$, where, σ is diagonal matrix of mean of the original random variables, $\mathbf{X}$ and $\mathbf{J}_{\mathbf{Y},\mathbf{X}}$ is the Jacobian matrix given by $\mathbf{J}_{\mathbf{Y},\mathbf{X}}^{\mathrm{t}} = \{\sigma\mathbf{TE}\}^{-1}$. Here $\mathbf{E}^2$ is the diagonal matrix of eigenvalues involved in the transformation.

It is believed that the above descriptors are of significant interest in modelling the optimal earthquake inputs. Finally, we wish to add that the procedure developed herein has the inherent capability to take into account any uncertainties that may exist in specifying the structure properties as well as permissible response levels.

4. Numerical results and discussions

4.1. Example 1: nonlinear singly supported sdof system

Herein, we demonstrate the procedures developed in the previous two sections for deriving critical stochastic excitations for a simple nonlinear sdof system under uniform ground motion. Thus we consider the steel frame studied in Part 1 of this paper (see Fig. 1). The structure is assumed to have spring stiffness $k_1 = k_2 = k/2$, $\alpha_1 = \alpha_2 = \alpha/2$ and damping $c_1 = c_2 = c/2$ with both the support points, A and B are taken to suffer identical ground motion $\ddot{x}_g(t)$. Under these simplifications, the unknown of the optimization is the psd function of $\ddot{w}_g(t)$ and the number of random variables involved in the reliability calculations reduces to $2N_f + 1$ $(R, \{A_n, B_n\}_{n=1}^{N_f})$. The present example represents a special case of the formulations developed in the previous two sections and, therefore, the details are omitted. The structure is taken to have a span length $L = 9.14\,\mathrm{m}$, height $h = 5.49\,\mathrm{m}$ and modulus of elasticity $E = 2.10 \times 10^{11}\,\mathrm{N/m^2}$. This leads to a spring stiffness $k = 4.67 \times 10^5\,\mathrm{N/m}$. The natural frequency of this structure is computed as 2.07 Hz and damping ratio, ζ is taken as 0.03. The load carrying capacity, that is based on the force in the spring, is modelled as a normal random variable with mean $\mu_R = 3.75 \times 10^4\,\mathrm{N}$ and standard deviation, $\sigma_R = 3.75 \times 10^3\,\mathrm{N}$. The frame structure is assumed to be located at a firm soil site and is analyzed under horizontal ground motion $\ddot{x}_g(t)$. As in Part 1 of this paper, it is assumed

that $E_0 = 1.45\,\mathrm{m}^2/\mathrm{s}^4$ and $n_0^+ = 1.64/\mathrm{s}$. This leads to $E_2 = 153.96\,\mathrm{m}^2/\mathrm{s}^6$ which, in turn, implies that the expected peak ground acceleration is about $0.44g$. The frequency bandwidth, (ω_0, ω_c) is taken as (0, 25.00) Hz. The increase of entropy rate, $\Delta\bar{H}_W$, from a reference white noise of intensity parameter $S_0 = 0.02\,\mathrm{m}^2/\mathrm{s}^3$, was computed to be 0.63. In the response surface calculations, a fourth-order Runge–Kutta method is used for numerical integration of the equation of motion. The parameters δ_1 and δ_2 that appear in the computation of the Hasofer–Lind reliability index algorithm are taken to be $\delta_1 = \delta_2 = 0.001$ and δ_3 was taken to be 10^{-6}. The constant f involved in the response surface fitting is taken as 3. This value was found to give a good match of critical psd function of $\ddot{w}_g(t)$, for the linear structure ($\varepsilon/\omega^2 = 0$) and with $e(t) = 1$, compared with that computed in example 1 of Part 1 of this paper. In fitting the response surface, the number of iterations to meet the convergence requirements was seen to be less than 10. The main optimization loop was initiated with alternative starting solutions and it was invariably found in each case that the final optimal solution was identical. The numerical results are obtained for different values of the nonlinearity parameter ε/ω^2. Table 1 summarizes the constraints scenarios considered. The results of this example are presented in Figs. 2–4. Fig. 2(a) shows the critical psd function of $\ddot{w}_g(t)$, for alternative values of ε/ω^2 for case 1. Similar results for constraints scenario 2 are presented in Fig. 2(b). Fig. 3(a) shows the amplitude spectrum of the ground acceleration, $\ddot{x}_g(t)$, at the design point, for $\varepsilon/\omega^2 = 0/\mathrm{m}^2$, while, similar results for $\varepsilon/\omega^2 = 1.00/\mathrm{m}^2$ are presented in Fig. 3(b). The sensitivity indices, $\gamma_i, i = 1, 2, ..., 4N_f$, are shown in Fig. 4(a) and (b). From results that are presented for this example, it is observed that the broad feature of critical psd functions for alternative constraints scenarios resemble the features that have been already observed for linear systems. Furthermore, as must be expected, with increases in values of μ_R, the critical β_{HL} increases and the associated P_{f_0} decreases. For example, with $\varepsilon/\omega^2 = 1.00/\mathrm{m}^2$, β_{HL} was computed to be 2.65, 3.15, 3.57, 3.94 and 4.46 when μ_R was taken to be 3.00, 3.38, 3.75, 4.13 and 4.50 kN, respectively. Focusing our attention on the influence of structural nonlinearity on the critical input characteristics, the following observations are made:

(1) The results corresponding to the first constraint scenario (case 1) shown in Fig. 2(a), clearly demonstrate the emergence of a secondary peak in the critical excitation psd function near the frequency close to three times the linear structure natural frequency. This characteristic is consistent with behavior of structures having cubic stiffness characteristic that is widely studied in the existing literature. Referring to Fig. 2(a), it can be observed that with increasing values of ε/ω^2, the secondary peak in the critical psd function climbs up while peak at the primary resonance frequency decreases.

Table 1
Nomenclature combinations of constraints used

	Constraints imposed	
Case	Singly supported sdof system	Multi-supported sdof system
1	E_T & n_0^+	E_x, n_{0x}^+, E_y, n_{0y}^+, σ_{AC} & σ_{AD}
2	E_T, n_0^+ & $\Delta\bar{H}_W$	E_x, n_{0x}^+, E_y, n_{0y}^+, σ_{AC}, σ_{AD}, $\Delta\bar{H}_{Wx}$ & $\Delta\bar{H}_{Wy}$

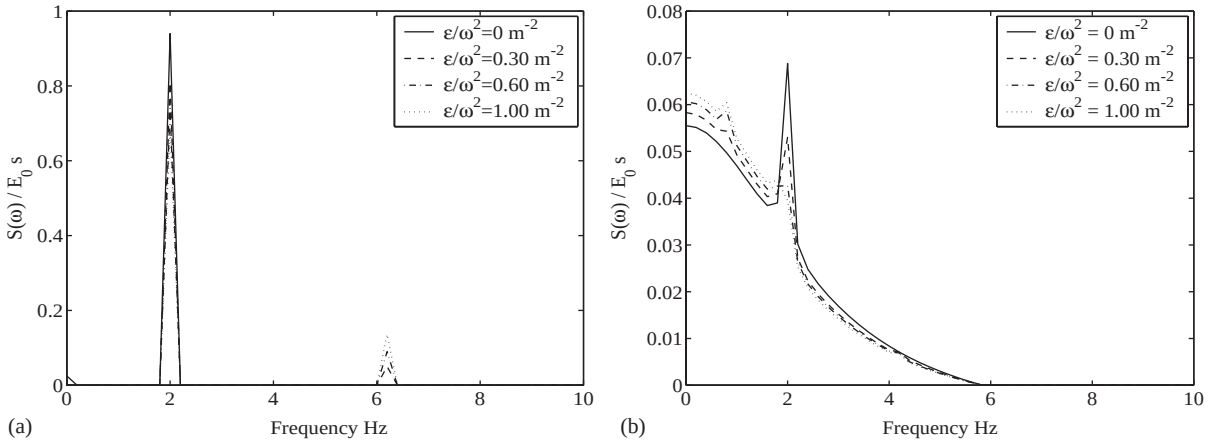

Fig. 2. Example 1: psd of $\ddot{w}_g(t)$. (a) Case 1, (b) case 2.

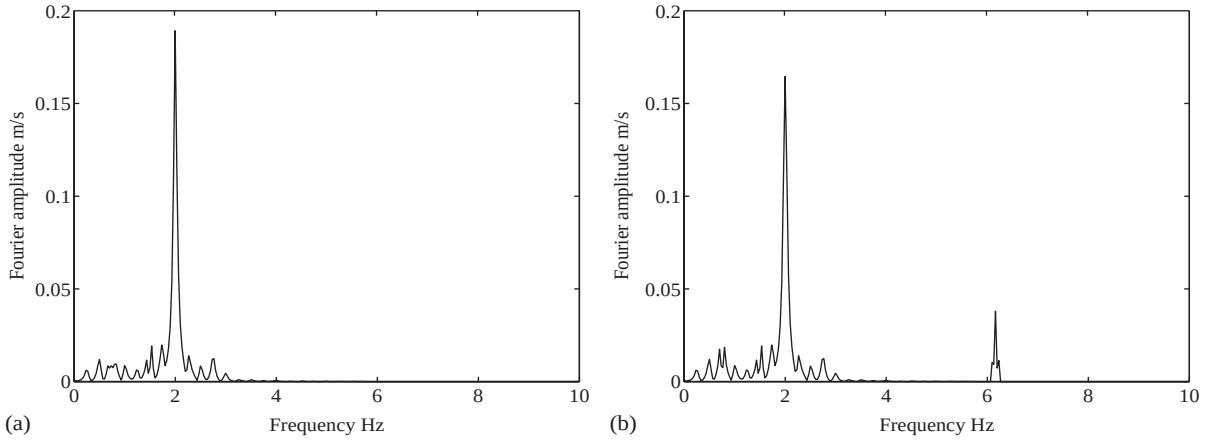

Fig. 3. Example 1, case 2: $\ddot{x}_g(t)$ at the design point. (a) $\varepsilon/\omega^2 = 0/\mathrm{m}^2$, (b) $\varepsilon/\omega^2 = 1.00/\mathrm{m}^2$.

(2) For the case of constraint scenario 2, where, additional constraint on entropy rate is brought in, the psd function of the critical excitation does not show the secondary peak at three times the natural frequency of the linear structure. This points towards a stronger influence that entropy rate constraint has on the characteristics of the psd of the critical excitation. Notwithstanding this, it is of interest to observe that the spectrum of excitation at the check point (Fig. 3(b)), indeed, reveals an additional peak at a frequency equals to three times the linear structure natural frequency. A similar observation can also be made in the plots of sensitivity factors (Fig. 4(b)) wherein, γ_i is shown to display notable fluctuations near the frequency that is three times the linear structure natural frequency.

(3) It is seen that the deterministic input excitation (a time history) at the check point is narrow band in nature with most of its energy concentrated at the structure natural frequency, see Fig. 3(a). Upon increasing the nonlinearity term, ε/ω^2, the design input gains amplitudes at

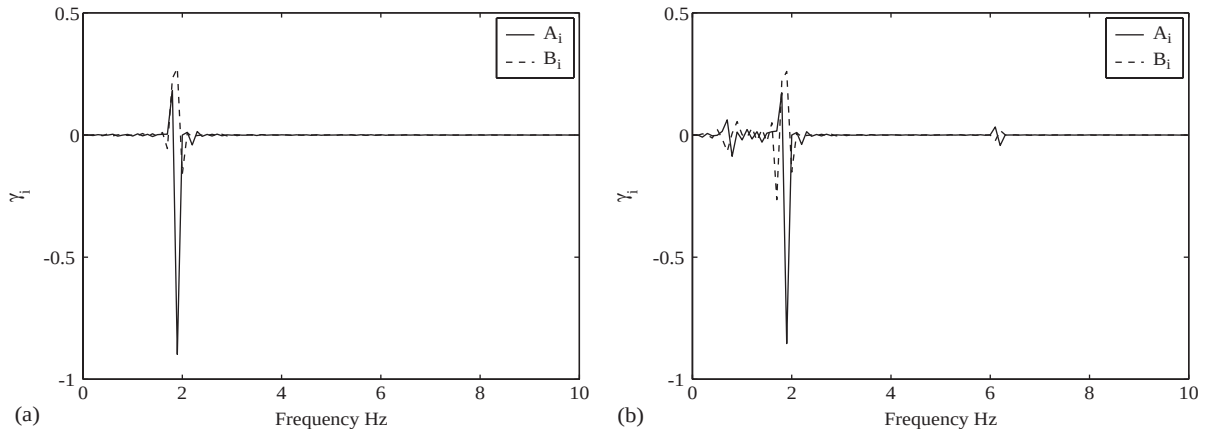

Fig. 4. Example 1, case 2: sensitivity indices γ_i, $i = 1, 2, \ldots, N_f$. (a) $\varepsilon/\omega^2 = 0/\mathrm{m}^2$, (b) $\varepsilon/\omega^2 = 1.00/\mathrm{m}^2$.

frequencies that are not the structure natural frequency (see Fig. 3(b)). Furthermore, the maximum displacement responses produced by the critical input compare well with those computed when the structure is subjected to the deterministic input at the check point. These values were computed to be 0.071, 0.059, 0.049 and 0.044 m from the critical input and to be 0.069, 0.058, 0.047 and 0.043 m from the deterministic time history for the nonlinearity parameter ε/ω^2 taken as 0, 0.30, 0.60 and $1.00/\mathrm{m}^2$, respectively.

(4) From the computation of the sensitivity of β_{HL} due to changes in the values of the constraints and envelope parameters, it is seen that β_{HL} is more sensitive to the entropy rate and the energy constraints, compared to the zero crossing rate constraint. The reliability index is less sensitive to the envelope parameters, α_1 and α_2. For example, for $\varepsilon/\omega^2 = 1.00/\mathrm{m}^2$, the percentage changes of β_{HL} are computed to be 0.93, 0.42, 3.21, 0.03 and 0.07 due changes of 1% in the parameters $E_T, n_0^+, \Delta\bar{H}_W$, α_1 and α_2, respectively.

(5) It is observed that the critical β_{HL} increases with increase in strength of the structure nonlinearity. The results on notional probability of failure corroborate the trends observed in β_{HL}. For example, for case 2, β_{HL} was computed to be 2.51, 2.97, 3.32 and 3.57, while P_{f_0} was 6.0366×10^{-3}, 1.4890×10^{-3}, 4.5009×10^{-4} and 1.7849×10^{-4} for ε/ω^2 taken as 0, 0.30, 0.60 and $1.00/\mathrm{m}^2$, respectively.

(6) One of the key assumptions made in the present study is that the minimization of reliability index implies the maximization of the true failure probability. Given that the true failure probability is not known exactly, it becomes important to verify that the assumption made in the study is indeed valid. To achieve this, Monte Carlo simulations of the structure failure probability, when the system is driven by its critical excitation, have been made using 6000 samples for different values of ε/ω^2. This has involved the generation of an ensemble of excitation time histories compatible with the critical psd functions predicted by the proposed procedure. The failure probability for $\varepsilon/\omega^2 = 0$, 0.3, 0.6 and 1.0 were estimated to be 9.1432E-03, 2.7436E-03, 6.7968E-03 and 2.7384E-04. respectively. One can compute notional reliability indices associated with these "true" failure probabilities and these indices turn out to be 2.36, 2.78, 3.20 and 3.46. These numbers compare reasonably well with the reliability indices computed using response surface method (viz., 2.51, 2.97, 3.32 and 3.57). This lends credence

to the expectation that an increase in the true failure probability implies a decrease in the reliability index.

4.2. Example 2: nonlinear multi-supported sdof system

Here we re-consider the example structure studied in the preceding section with the modification that the supports A and B (Fig. 1) now suffer differential ground motions. In the numerical calculations it is assumed that the frequency range for $\ddot{x}_g(t)$ and $\ddot{y}_g(t)$ is (0–25.00) Hz and $N_f = 20$. Therefore, the total number of random variables involved in computing critical earthquake excitations turns out to be 81. The set of input frequencies $\{\Omega_n\}_{n=1}^{N_f}$ in the series representations (see Eq. (5)) were chosen such that discrete harmonic components were present at ω, 2ω and 3ω, where ω is the natural frequency of the frame structure. The parameters of the envelope functions are taken to be $\alpha_{x_1} = \alpha_{y_1} = 0.13$, $\alpha_{x_2} = \alpha_{y_2} = 0.50$, and $A_{0x} = A_{0y} = 2.17$. This implies a duration of about 30 s for both the accelerations. The quantities that reflect constraints that are relevant in computing the critical earthquake loads are taken to be $E_{0x} = 1.45\,\mathrm{m}^2/\mathrm{s}^4$ and $E_{0y} = 1.45\,\mathrm{m}^2/\mathrm{s}^4$. This leads to $E_{Tx} = E_{Ty} = 11.40\,\mathrm{m}^2/\mathrm{s}^4$. The dominant input frequencies are taken to be $n_{0x}^+ = n_{0y}^+ = 1.64/\mathrm{s}$ and thus $E_{2x} = E_{2y} = 153.96\,\mathrm{m}^2/\mathrm{s}^6$. This, in turn, implies that the expected peak values of both the accelerations is about $4.35\,\mathrm{m}/\mathrm{s}^2$ ($0.44g$). The increases of entropy rate for both ground accelerations from a reference white noise of intensity $0.02\,\mathrm{m}^2/\mathrm{s}^3$ were taken to be $\Delta\tilde{H}_{Wx} = \Delta\tilde{H}_{Wy} = 0.63$.

The results of this example are presented in Figs. 5–10. In general, the features of the critical inputs were found similar to those observed in Example 1. Apart from this, the following observations are made: For case 1 and for the linear structure (i.e. $\varepsilon/\omega^2 = 0/\mathrm{m}^2$), the critical input auto psd functions are seen to be resonant with all their power concentrated near the linear structure natural frequency. Similarly, the critical coherency function has the same characteristic. Upon inclusion of nonlinearity, it is observed that the auto psd functions gain a secondary peak at twice the linear structure natural frequency, that indicates that the system is parametrically excited due to the presence of the nonlinearity. Furthermore, a secondary peak, at a frequency that is around three times the linear structure natural frequency, is also observed (see Fig. 5). The critical coherency function, in this case, possesses a secondary peak at twice the linear structure natural frequency, in addition to, the primary peak at the linear structure natural frequency, and with zero phase angle (see Fig. 6). These characteristics are also observed in the spectrum of the ground accelerations at the design point and also the sensitivity factors as can be seen in Figs. 9 and 10. Upon imposition of the entropy rate constraint (case 2), the critical auto psd functions of the ground accelerations are seen to possess a secondary peak at twice the linear structure natural frequency. The parametric excitation effect is also observed in the cross coherency function, which increases remarkably upon increasing the nonlinearity term, ε/ω^2 (see Fig. 8). Furthermore, the influence of the structure nonlinearity, can be observed, clearly, in the plots of the sensitivity factors, $\{\gamma_i\}_{i=1}^{4N_f}$, shown in Fig. 10(b), where, these factors show remarkable fluctuations at frequencies away from linear structure frequency, when nonlinearity is brought in. It is of interest, to observe here, that the critical phase angle is neither in phase nor out of phase. Finally, it may be noted that the critical auto-psd functions of $\ddot{w}_g(t)$ and $\ddot{v}_g(t)$ (Fig. 7) show broadly similar features; similar observation also holds good for the Fourier amplitude spectra of $\ddot{x}_g(t)$ and $\ddot{y}_g(t)$ (Fig. 9). The actual differences that exist between excitations at left and right supports are not discernable

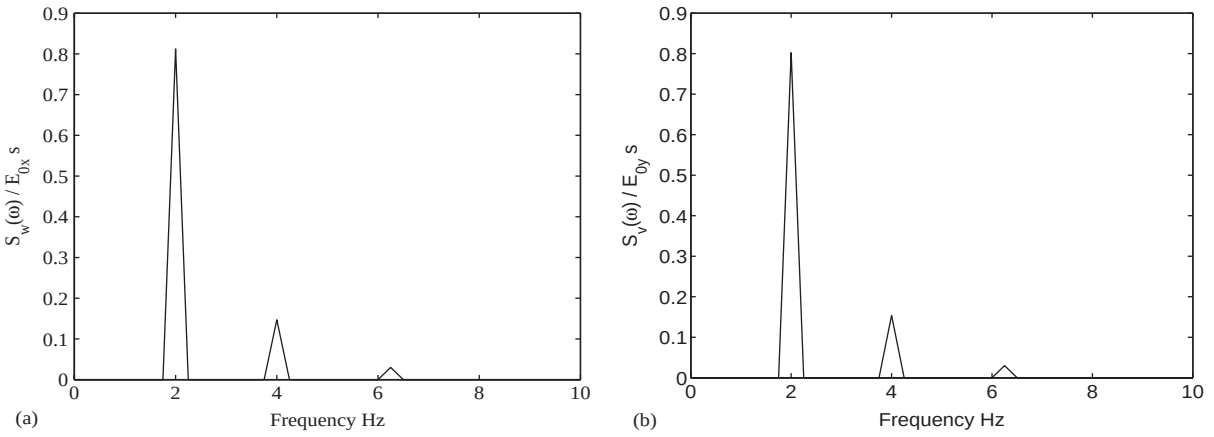

Fig. 5. Example 2, case 1: critical psd function. (a) $\ddot{w}_g(t)$, (b) $\ddot{v}_g(t)$, $\varepsilon/\omega^2 = 1.00/\mathrm{m}^2$.

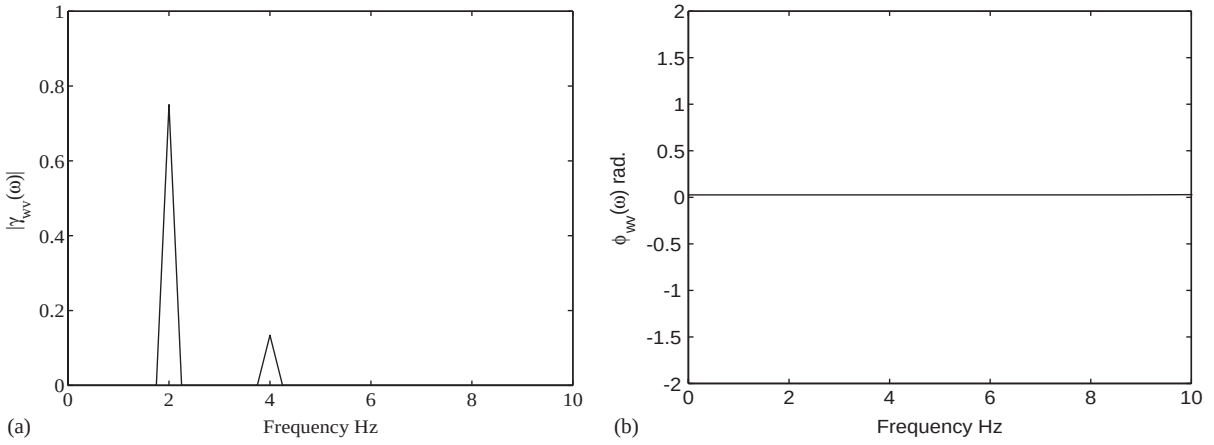

Fig. 6. Example 2, case 1: cross psd function. (a) $|\gamma_{wv}(\omega)|$, (b) $\phi_{wv}(\omega)$, $\varepsilon/\omega^2 = 1.00/\mathrm{m}^2$.

from these plots. These similarities are to be expected given the symmetry of structure ($k_1 = k_2; \alpha_1 = \alpha_2; c_1 = c_2$) and symmetry in excitation characteristics ($e_x(t) = e_y(t); E_{0x} = E_{0y}; E_{2x} = E_{2y}; \Delta\bar{H}_{Wx} = \Delta\bar{H}_{Wy}$). The mild dissimilarity in these plots is due to the fact that the optimization variable here involves force in the left spring. It is nevertheless important to note that the spatial variability in support motions are characterized through the coherence functions shown in Fig. 8(a) and (b).

5. Conclusions

A new definition for random critical earthquake excitations for nonlinear singly supported or multiply supported structures has been introduced in this paper. These excitations are tailored to

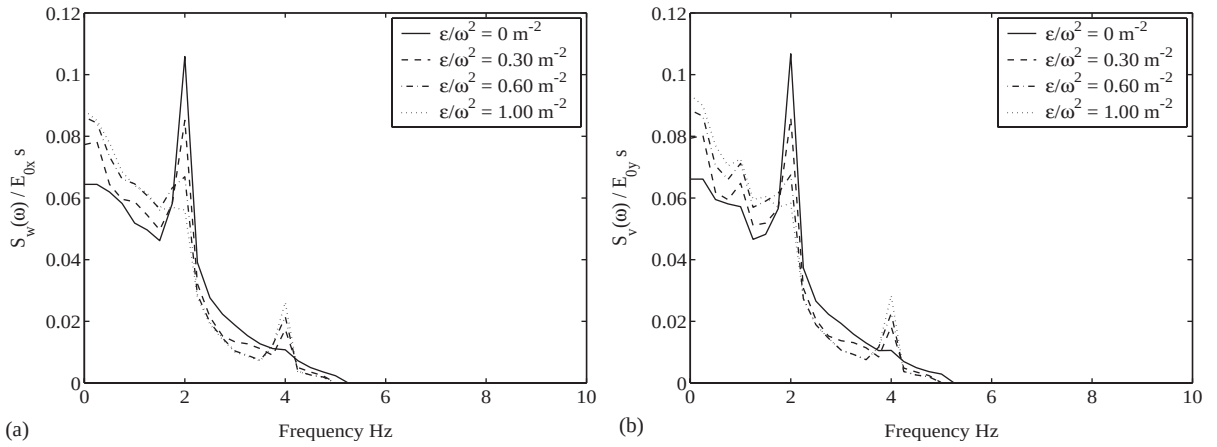

Fig. 7. Example 2, case 2 : critical psd function. (a) $\ddot{w}_g(t)$, (b) $\ddot{v}_g(t)$.

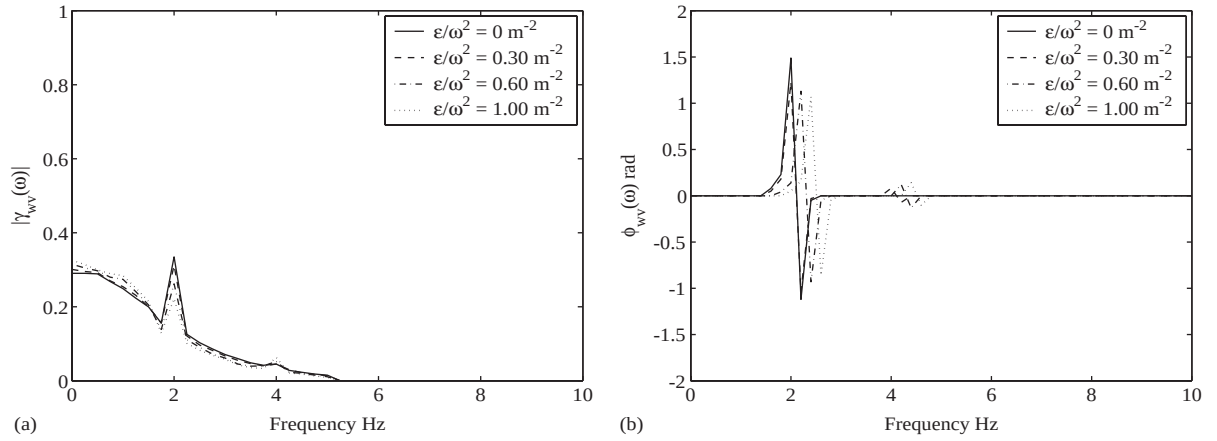

Fig. 8. Example 2, case 2: cross psd function. (a) $|\gamma_{wv}(\omega)|$, (b) $\phi_{wv}(\omega)$.

minimize the Hasofer–Lind reliability index with respect to performance functions involving admissible limits on extreme values of response displacement/internal forces over a specified time interval. These indices, in turn, are evaluated approximately by employing response surface modelling. The algorithm proposed in this paper has the capability of accounting for nonstationarity of the excitations as well as uncertainties in the system parameters. The excitations are taken to satisfy constraints on total average energy, zero crossing rate, entropy rate and other positivity and bounding requirements that are of mathematical nature. The proposed approach offers a new perspective in critical earthquake excitation modelling for nonlinear structures, especially in relation to the existing models that often employ methods of equivalent linearization in handling the problem. Furthermore, the formulation of critical excitations in terms of optimal reliability indices, as reported in this study, leads to a set of input-response

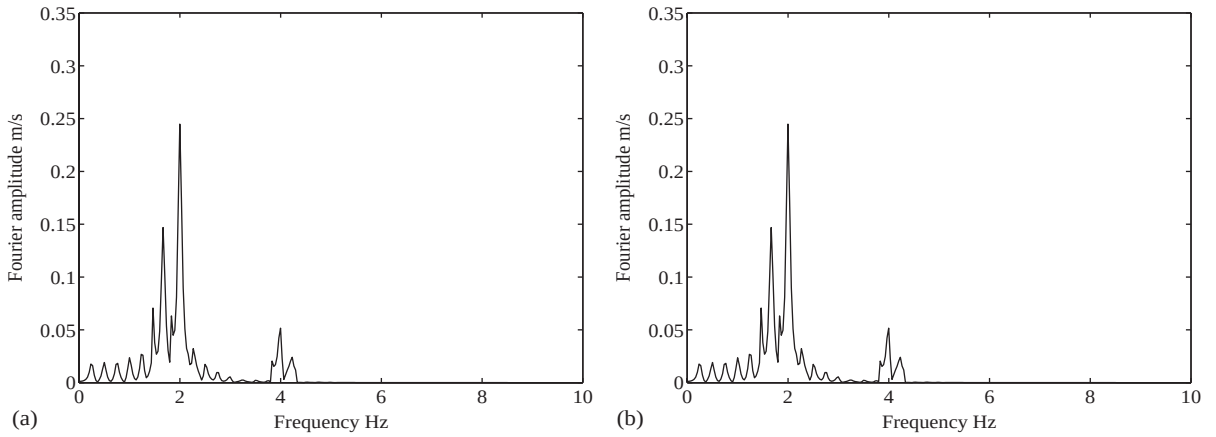

Fig. 9. Example 2, case 2: inputs at the design point. (a) $\ddot{x}_g(t)$, (b) $\ddot{y}_g(t)$, $\varepsilon/\omega^2 = 1.00/\mathrm{m}^2$.

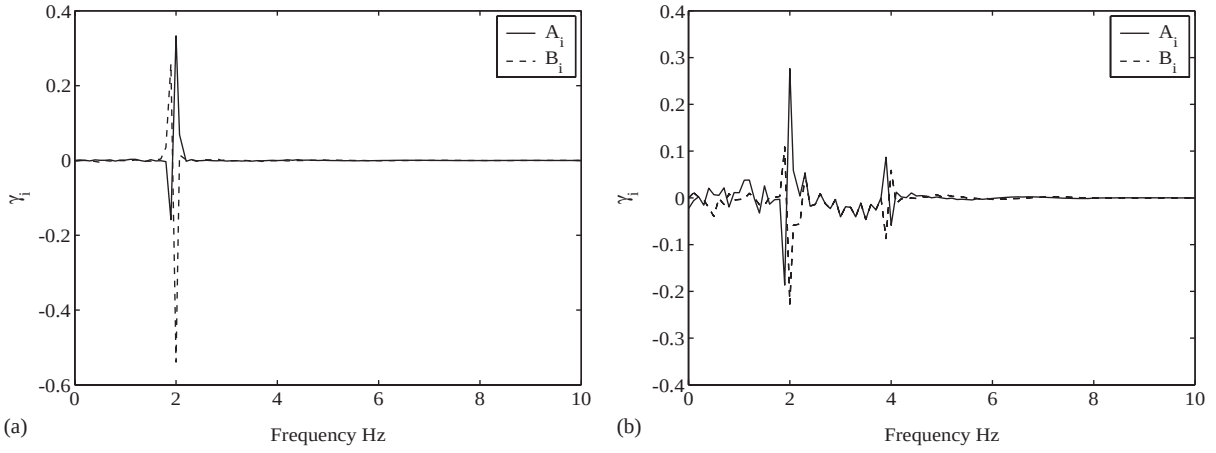

Fig. 10. Example 2, case 2: sensitivity indices for $\ddot{x}_g(t)$. (a) $\varepsilon/\omega = 0/\mathrm{m}^2$, (b) $\varepsilon/\omega^2 = 1.00/\mathrm{m}^2$.

descriptors that are of significant importance in modelling optimal earthquake inputs for nonlinear structures. The illustrative examples that are presented on nonlinear singly supported and doubly supported oscillators clearly demonstrate the influence that the structural nonlinearity has on the nature of critical input psd functions.

It is important to note that the proposed method employs first-order reliability methods and, therefore, it automatically carries with it all the limitations of these methods. Also, in the present form of its implementation, the method does not take into account the possible existence of multiple design points. The new formulations developed in the present study on reliability-based critical excitations have been illustrated with respect to fairly simple structures. The study has focussed on developing critical excitations associated with single response variables. Further work, that combines response surface modelling with methods of system reliability analysis, needs

to be carried out to extend the scope of the present formulation to consider more than one response variable in characterizing the critical excitations. Here one would aim to maximize the lower bound on the system probability of failure. Furthermore, the scope of the critical excitation models can be significantly improved if the nonstationarity in frequency content of earthquake ground motions can be taken into account. Similarly, the long-range uncertainties associated with the earthquake phenomenon can be taken into account by treating the constraints used in defining critical excitations as being random in nature. Also, given the significant interest in earthquake engineering on controlled inelastic behavior of engineering structures during strong motion earthquakes, it is of much interest to extend the scope of the critical excitation models to large-scale engineering structures with hysteretic nonlinearities. This can be achieved by integrating tools of nonlinear optimization with finite element modelling and response surface methods. In the treatment of spatially varying earthquake load models (Section 2) the complex-valued cross-psd functions between the excitation components at different locations plays an important role. In the published literature there exist several models for these spectra based on the examination of recorded data and study of seismic wave propagation phenomenon. The development of critical psd function matrix models can be improved upon by including the known features of cross-psd functions as suitable constraints. These issues are presently under study by the present authors. The problems of constrained nonlinear optimization that underlie the study reported in this two-parts paper have been solved using sequential quadratic programming tools. Generally, these methods are not guaranteed to give the global optimal solutions. In the present study, this issue has been examined essentially numerically. In fact, it was generally observed that initiating numerical optimization steps with different starting guesses lead to the same optimal solutions. Furthermore, these solutions were considered acceptable since they displayed qualitatively the features that could be explained in a consistent manner. In this context, the use of alternative powerful optimization tools such as those based on genetic algorithms, should be of interest. This, however, requires further work.

Acknowledgements

The work reported in this paper has been partly supported by funds from the Department of Science and Technology, Government of India.

References

[1] A.M. Abbas, C.S. Manohar, Reliability-based critical earthquake load models. Part 1: linear structures, *Journal of Sound and Vibration* 287 (4 + 5) (2005) 865–882; doi:10.1016/j.jsv.2004.12.002.

[2] R.N. Iyengar, Worst inputs and a bound on the highest peak statistics of a class of non-linear systems, *Journal of Sound and Vibration* 25 (1) (1972) 29–37.

[3] R.F. Drenick, The critical excitation of nonlinear systems, *Journal of Applied Mechanics* 18 (1977) 333–336.

[4] A.J. Philippacopoulos, P.C. Wang, Seismic inputs for nonlinear structures, *Journal of Engineering Mechanics* 110 (5) (1984) 828–836.

[5] B.D. Westermo, The critical excitation and response of simple dynamic systems, *Journal of Sound and Vibration* 100 (2) (1985) 233–242.

[6] A.A. Pirasteh, J.L. Cherry, J.A. Balling, The use of optimization to construct critical accelerograms for given structures and sites, *Earthquake Engineering and Structural Dynamics* 16 (1988) 597–613.
[7] R. Ravi, Random Earthquake Response Analysis of Multiply Supported Nuclear Power Plant Secondary Systems, MSc Thesis, Department of Civil Engineering, Indian Institute of Science, 1997.
[8] C.H. Srinivas, Critical Cross Power Spectral Density Models for Earthquake Loads on Multi-supported Structures, MSc Thesis, Department of Civil Engineering, Indian Institute of Science, 1998.
[9] I. Takewaki, Probabilistic critical excitation for MDOF elastic–plastic structures on compliant ground, *Earthquake Engineering and Structural Dynamics* 30 (2001) 1345–1360.
[10] I. Takewaki, Critical excitation for elastic–plastic structures via equivalent linearization, *Probabilistic Engineering Mechanics* 17 (2002) 73–84.
[11] L. Faravelli, Response-surface approach for reliability analysis, *Journal of Engineering Mechanics* 115 (12) (1989) 2763–2781.
[12] C.G. Bucher, U. Bourgund, A fast and efficient response surface approach for structural reliability problem, *Structural Safety* 7 (1990) 57–66.
[13] M.R. Rajashekhar, B.R. Ellingwood, A new look at the response surface approach for reliability analysis, *Structural Safety* 12 (3) (1994) 205–220.
[14] A.H.S. Ang, W.H. Tang, *Probability Concepts in Engineering Planning and Design: Vol. II, Decision, Risk and Reliability*, Wiley, New York, 1984.
[15] A.D. Kiureghian, J.-B. Ke, Finite-element based reliability analysis of frame structures, *Proceedings, International Conference on Structural Safety and Reliability* (*ICOSSAR*), Vol. 1, Kobe, Japan, 1985, pp. 395–404.